Earth and Space Science

TECHNICAL REPORTS: METHODS
10.1029/2019EA000588

ScintPi: A Low-Cost, Easy-to-Build GPS Ionospheric Scintillation Monitor for DASI Studies of Space Weather, Education, and Citizen Science Initiatives

F. S. Rodrigues[1] **and A. O. Moraes**[2]

[1]The University of Texas at Dallas, Richardson, TX, USA, [2]Instituto de Aeronáutica e Espaço-IAE, São Paulo, Brazil

Key Points:

- We propose a low-cost, easy-to-build GPS-based sensor (ScintPi) for ionospheric studies and educational and citizen science initiatives
- Comparisons with measurements provided by a collocated, commercial scintillation receiver are presented
- Results from short- and long-term observations confirm the ability of ScintPi to detect and monitor ionospheric irregularities

Correspondence to:
F. S. Rodrigues,
fabiano@utdallas.edu

Citation:
Rodrigues, F. S., & Moraes, A. O. (2019). ScintPi: A low-cost, easy-to-build GPS ionospheric scintillation monitor for DASI studies of space weather, education, and citizen science initiatives. *Earth and Space Science*, *6*, 1547–1560. https://doi.org/10.1029/2019EA000588

Received 5 FEB 2019
Accepted 3 JUL 2019
Accepted article online 11 JUL 2019
Published online 13 AUG 2019

Abstract We report the proposal and results of a low-cost, easy-to-build GPS-based sensor for detection and monitoring ionospheric irregularities through the detection of amplitude scintillation. The system is based on the Raspberry Pi single-board computer combined with an Adafruit Ultimate GPS peripheral, which is capable of measuring (at 10-Hz rate) the intensity of the L1 signals transmitted by GPS satellites. We introduce and discuss results of short- and long-term observations obtained with a prototype of this system deployed in Presidente Prudente, a low magnetic latitude site in Brazil. The deployment and observations were carried out to test the ability of the system to detect ionospheric scintillations and, therefore, monitor the occurrence of ionospheric irregularities associated with equatorial spread *F*. Our results show that this low-cost sensor is indeed capable of detecting scintillation events associated with equatorial spread *F*. Comparison with simultaneous, collocated measurements made by a commercial scintillation monitor are also presented. The joint observations allowed us to quantify the performance of the low-cost monitor and to identify sources of potential limitations. While the sensor cannot (and it was not intended to) substitute commercial scintillation monitors, the low cost allows its use in studies of ionospheric irregularities (space weather) that require observations made by distributed arrays of small instruments (DASI). Furthermore, the simplicity of the sensor design stimulates its use in educational and citizen science initiatives.

Plain Language Summary It is well recognized that progress in space sciences can benefit from observations made by distributed arrays of instruments. Additionally, the value of integrated research and education as well as citizen science initiatives became more evident in the past few years. To support such efforts, we propose and investigate the use of off-the-shelf, inexpensive electronic devices to create a sensor capable of providing useful information about the space environment near Earth as well as being used in educational activities. We present results of a low-cost, easy-to-build instrument (ScintPi) capable of providing information about irregularities in the density of the Earth's ionosphere. Ionospheric irregularities are known to affect the performance of radio systems used for navigation, communication, and remote sensing. The components of the instrument are readily available and commonly used by hobbyists. Despite its simplicity, we show that this instrument is capable of providing useful information about the state of the ionosphere. More importantly, the low cost of this instrument allows its use in geospace studies that require a dense regional network of measurements, educational programs, and citizen science initiatives.

1. Introduction

The Earth's ionosphere is a region of the upper atmosphere that is located above approximately 50-km altitude. It is characterized by a relatively high density of free ions and electrons, which are created, in most part, by solar photoionization of neutral atmospheric species (Kelley, 2009). The ionosphere can also be described as a weakly ionized, magnetized plasma. Under the action of different types of plasma instabilities, temporal and spatial fluctuations in the ionospheric electron density develop. These irregularities have been observed at high and middle latitudes but are known to occur more frequently, and with larger amplitudes, at low latitudes (Aarons, 1982).

The study of the ionosphere is motivated by a better understanding of fundamental physical processes controlling the dynamics and energetics of the geospace plasma and its coupling with the other regions including the magnetosphere and neutral atmosphere. Fundamental studies of the ionosphere are also motivated by a better understanding of the conditions leading to plasma instability growth and irregularity

development. Ionospheric irregularities are an important component of space weather, which refers to conditions on the space near Earth that can influence the performance and reliability of technological systems and endanger human life or health (e.g., Baker & Lanzerotti, 2016).

The ionosphere can be studied experimentally using in situ and remote sensing sensors on satellites and rockets (Kelley et al., 1980; Rino et al., 1981) and using ground-based radio (Farley, 1991; Isham et al., 2000) and optical instrumentation (Makela, 2006; Tinsley & Bittencourt, 1975). In recent years, however, it has become more recognized that distributed arrays of small instruments (DASI) can provide new information and help advance understanding about the state of the space environment near Earth (e.g., Coupling, Energetics and Dynamics of Atmospheric Regions, 2010; National Research Council, 2006). Additionally, recent studies have shown the benefit of crowdsourcing and engagement of citizen scientists in studies of the space environment (Barnard et al., 2014; Frissell et al., 2014; Knipp, 2015; Kosar et al., 2018; MacDonald et al., 2015; Perry et al., 2018). These trends motivate the study of new, low-cost instruments capable of providing useful observations.

Of particular importance to this report has been the use of GPS signals for remote sensing of the integrated background ionospheric electron density and irregularities. The ionospheric plasma has an index of refraction that depends on electron density and on the frequency of the electromagnetic wave propagating through the medium. Variations in electron density associated with ionospheric irregularities cause the diffraction of radio waves transmitted by satellites to ground receivers. The interference of the diffracted wavefronts cause fluctuations (scintillation) in the amplitude and phase of signals observed by a static (or moving) receiver (Kintner et al., 2007). While scintillation can affect the performance of Global Navigation Satellite Systems receivers (Skone et al., 2001), it can also be used to as tracers of ionospheric irregularities (Beach & Kintner, 2001). The birefractive nature of the ionospheric plasma also allows the use of multiple coherent signals with different frequencies transmitted by satellites to infer information about the ionospheric total electron content (Jakowski, 1996). Multiple dual-frequency GPS receiver measurements can even be used to "image" the ionosphere (e.g., Bust & Mitchell, 2008).

While single-frequency GPS receivers cannot provide direct information about the ionospheric total electron content, they are less expensive and can still provide information about ionospheric irregularities. Here, we present results of an effort to evaluate the application of an inexpensive, single-frequency GPS unit (Adafruit Ultimate GPS) connected to a low-cost, readily available single-board computer (Raspberry Pi) for studies of ionospheric irregularities. The parts used in this low-cost sensor are off-the-shelf and can be easily purchased either online or from an electronics store at a total cost of about US$ 100.00. The proposed system, which we refer to as "ScintPi," is not intended to replace commercial ionospheric scintillation receivers. We envision, however, the use of the system in regional, dense arrays of sensors to assist scientific studies related to ionospheric irregularity generation, development, and decay. We also anticipate its use in educational and citizen science initiatives related to space sciences.

This report is organized in the following order. In section 2, we describe the proposed system and its features and provide an estimate of the current costs. In section 3, we provide details of an extensive observation campaign and analysis carried out to evaluate the ability of the system to identify low-latitude ionospheric irregularities. In section 4, we present and discuss results associated with short- and long-term observations. We also discuss results of a comparison between ScintPi observations and those made by a collocated, commercial scintillation monitor (Septentrio PolaRx5S). Strengths and weaknesses of ScintPi are identified and described. Finally, in section 5, we provide a summary of our results and potential plans for the future.

2. Instrumentation

In an attempt to create a low-cost space science instrument that could be used in educational activities and to create new, useful sets of measurements, we investigated the use of an inexpensive, single-frequency GPS receiver that could be easily interfaced for acquisition and data collection.

The choice of GPS receiver was the Adafruit Ultimate GPS Breakout module (Adafruit, 2018). The Adafruit GPS module is built around the MediaTek MTK3339 chipset, which is described as high-performance single-chip GPS solution. MTK3339 includes on-chip complementary metal-oxide semiconductor (CMOS) radio frequency, digital baseband, and an ARM7 CPU. The low-power consumption (25 mW for acquisition and

18 mW for tracking) of the chipset makes it adequate for power sensitive applications including mobile phones and gaming devices. The GPS module is a 66-channel GPS receiver capable of tracking up to 22 satellites simultaneously and outputting GPS information, including L1 signal-to-noise ratio (SNR), at 10 Hz.

The GPS module comes with a built-in patch antenna, but it also provides a uFL connection for an external active (3 V) antenna. Detection and use of the external antenna are automatic. Since most GPS antennas use SMA connectors, a uFL to SMA adapter cable is needed. The GPS module uses the transistor-transistor logic serial communication to output information. The information sent by the module follows the National Marine Electronics Association (NMEA) message structure. Of relevance to our studies of ionospheric scintillation are information of date, time, receiver position, and intensity of the signals being tracked by the receiver that are available in the NMEA message. With respect to intensity, the NMEA message provides the field SNR (dB), which was taken to be an estimate of the L1 signal power. Later on, we show that this is indeed an acceptable proxy for the signal intensity.

Next, we selected a low-cost device that would be able to communicate with the GPS module and collect and store the GPS information. The device chosen was the Raspberry Pi 3 (RPi3) Model B. Raspberry Pi is a series of small single-board computers whose development aimed at promoting teaching of basic computer science in schools and developing countries (https://www.raspberrypi.org). The first generation of Raspberry Pi was released in February 2012, followed by several other versions with varying memory capabilities and support for peripheral devices. RPi3B features a 1.2-GHz 64-bit quad-core ARMv8 CPU and 1 GB of RAM. Additionally, the RPi3B has four USB ports, built-in 802.11n wireless LAN, built-in Bluetooth 4.1, 40 GPIO pins, HDMI and ethernet ports, and a micro-SD card slot.

The GPS module is connected to the RPi3 via a USB-transistor-transistor logic adapter cable. Software for communication (serial, NMEA) and data acquisition is straightforward and was written in Python. The software sets GPS measurements to be made at 10-Hz rate and collects information from the GPS receiver. Information that are relevant to ionospheric scintillation studies are written into daily data files that are saved in the RPi3 SSD card. The data files contain the following information for each tracked satellite: (1) universal time, (2) satellite identifier (SVID), (3) satellite azimuth angle, (4) satellite elevation, (5) SNR NMEA parameter for the L1 signal, GPS-computed (6) latitude, (7) longitude, and (8) altitude coordinates for the receiver.

One of the challenges of using an inexpensive GPS receiver such as the Adafruit Ultimate Breakout module is to determine the usefulness of the information provided to users via NMEA messages. Of particular importance to ionospheric scintillation studies is the SNR parameter that is provided with the NMEA message. The field SNR, which is often referred to as signal strength, is described as an integer value ranging from 00 to 99 that has units of decibels (dB). As part of this study we found that the Adafruit GPS limits the SNR parameter to a maximum value (52 dB). Therefore, the values provided by the receiver are limited not only in temporal resolution (one sample every 0.1 s) but are in amplitude resolution (1 dB) and a maximum value of 52 dB. This study investigated the ability of such receiver (and measurements) to identify ionospheric scintillation despite the limitations cited above.

Figure 1a shows an example of a lab setup where the GPS receiver is connected to the RPi3. The main components of the setup are indicated. As mentioned earlier, we refer to this scintillation monitor as ScintPi. Table 1 provides information about current costs of the parts used in the prototype. Note that we do not list the cost of an external GPS L1 antenna. The cost of single-frequency GPS antennas that could be used by ScintPi vary from a few tens to a few hundreds of U.S. dollars. In the next section we describe the antenna used in our tests. The antenna was available at the observation site along with a specialized commercial scintillation monitor, which allowed comparisons of the measurements.

3. Observational Setup

In order to evaluate the ability of ScintPi to detect scintillations and provide useful information about ionospheric irregularities, we deployed a prototype of the system and conducted an extensive campaign of observations.

The system was installed in Presidente Prudente (PPR, 22.1°S, 51.24°W, −16.8° dip latitude), a low magnetic latitude site in Brazil. The site was chosen due to its proximity of the nominal location of the equatorial

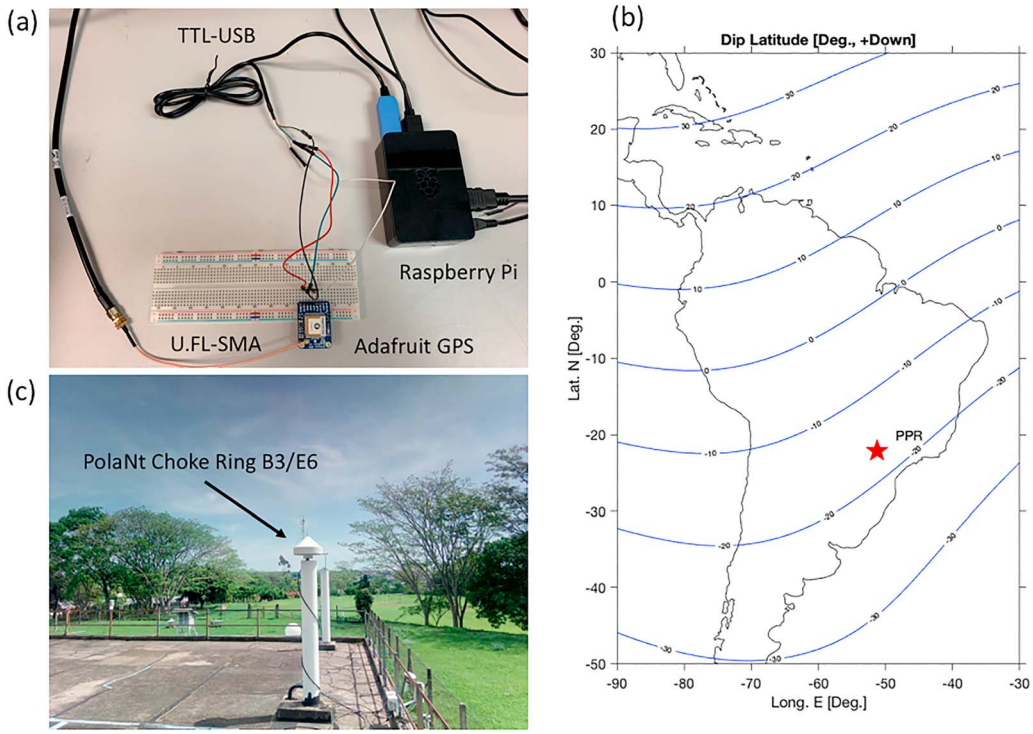

Figure 1. (a) Illustration of a ScintPi prototype setup. (b) Location of the observation site (Presidente Prudente, 22.1°S, 51.24°W, −16.8° dip latitude) in Brazil. Isolines of magnetic latitude are also shown for reference. (c) The PolaNt Choke Ring B3/E6 multifrequency antenna user for collocated, simultaneous observations made by ScintPi and Septentrio PolaRx5S at our observation site (Presidente Prudente) in Brazil. TTL = transistor-transistor logic.

ionization anomaly, where L-Band amplitude scintillation is expected to occur with a broad range of magnitudes. Figure 1b shows a map indicating the location of the observation site. Figure 1b also shows isolines of magnetic latitude for reference. The latitudes were computed using the International Geomagnetic Reference Field (IGRF) model for 15 June 2018 and an altitude of 350 km.

The choice of the PPR site for the field tests was also motivated by the availability of a commercial scintillation monitor, commonly used for ionospheric studies (Moraes, Muella, et al., 2017, Moraes, Costa, et al., 2017; Moraes et al., 2018; Vani et al., 2016). The commercial monitor is a Septentrio PolaRx5S, which is multifrequency Global Navigation Satellite Systems receiver capable of tracking signals from GPS, GLONASS, Galileo, BeiDou, IRNSS, QZSS, and SBAS. PolaRx5S outputs various scintillation indices including the amplitude scintillation index (S_4) computed for the GPS L1 C/A signal, which is of interest here for comparison with ScintPi scintillation estimates. The indices output by Septentrio are based on high precision, low-noise measurements of amplitude and phase made at a rate of 100 Hz. For the purpose of this study, the PolaRx5S measurements are used as reference, or true, values.

For an adequate comparison between ScintPi and PolaRx5S estimates of scintillation, measurements were made by both receivers using signals collected by the same antenna. The PolaNt Choke Ring B3/E6 is a multifrequency antenna and was used for the measurements. The signal received by the antenna was sent to the two receivers using a signal splitter. The antenna is equipped with low-noise amplifiers, and it is designed to mitigate multipath. Nevertheless, we use an elevation mask of 20° to avoid effects of multipath on our analyses. Figure 1c shows the antenna setup on the observation site (PPR).

Table 1
A Summary of the Costs Associated With the Parts Used to Assemble the ScintPi Prototype

Component	Unit cost (US$)	Quantity	Total cost (US$)
Raspberry Pi 3 Model B	35.00	1	35.00
USB to TTL cable	9.95	1	9.95
Adafruit ultimate GPS breakout	39.95	1	39.95
SMA to uFL adapter cable	3.95	1	3.95
Raspberry Pi 3 Model B case with fan	15.99	1	15.99
Total prototype cost (US$)			104.84

Note. The cost of an external antenna is not included in this summary. The cost of GPS antennas that could be used by ScintPi varies from a few tens to a few hundreds of U.S. dollars.

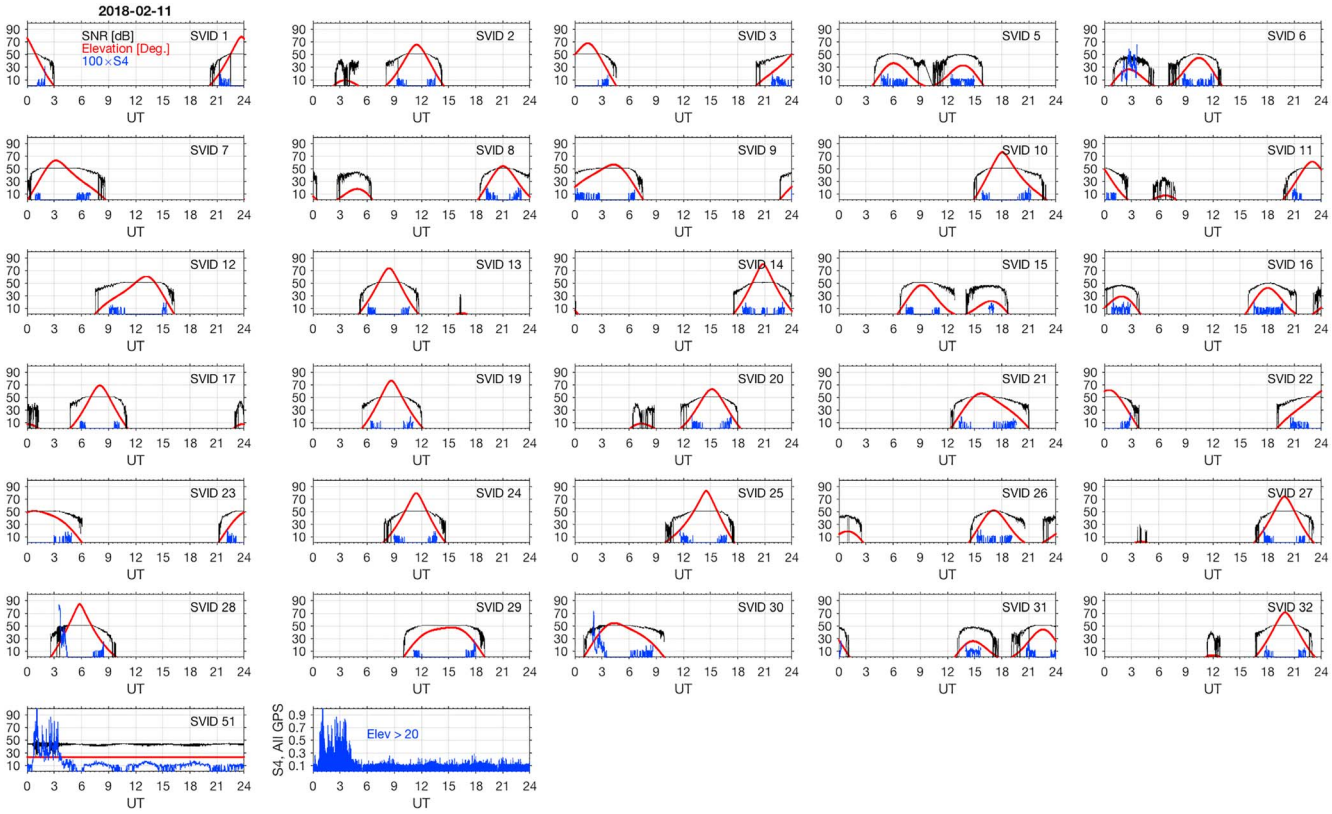

Figure 2. Example of observations made by ScintPi on 11 February 2018 (UT to LT + 3.5). SNR = signal-to-noise ratio.

Our campaign of observations in PPR started on 25 January 2018. For this report, we processed and analyzed all the observations made in 2018. The receiver operated nearly continuously, generating 333 days of observations. Data gaps were caused, in most cases, by electrical power outages at the site.

4. Results and Discussion

We now present and discuss the main results of a comprehensive analysis of the observations made by ScintPi. We start by providing and discussing examples of typical observations, followed by comparisons of ScintPi and PolaRx5S measurements. Then, we present and discuss results of long-term (~1 year) observations made by ScintPi.

4.1. Example of Typical Observations

Figures 2 presents an example of typical observations made by ScintPi. The observations are for 11 February 2018. Each panel shows the signal intensity (SNR) measured by ScintPi for a GPS satellite as a function of universal time (UT). The identifier number (SVID) of each satellite is indicated in the panels. Each panel also shows the elevation of the satellite and an estimate of the S_4 index, which is commonly used to identify ionospheric irregularities through amplitude scintillation (Kintner et al., 2007; Yeh & Liu, 1982). The S_4 index is only computed for signals from satellites with elevation greater than 20° to avoid signal fluctuations of nongeophysical origin (multipath).

As usual, the S_4 index is determined from the normalized variance of the GPS L1 signal intensity (I). For ScintPi, intensities were determined from the SNR values (in decibels) provided by the NMEA message: $I = 10^{\mathrm{SNR}/10}$. The ScintPi S_4 index is then estimated from $S_4 = \sigma_I/I$, where σ_I^2 and I are estimates of the variance and mean of the signal intensity, respectively. These estimates are computed using intensity samples measured over an interval of 1 min (total of 600 samples).

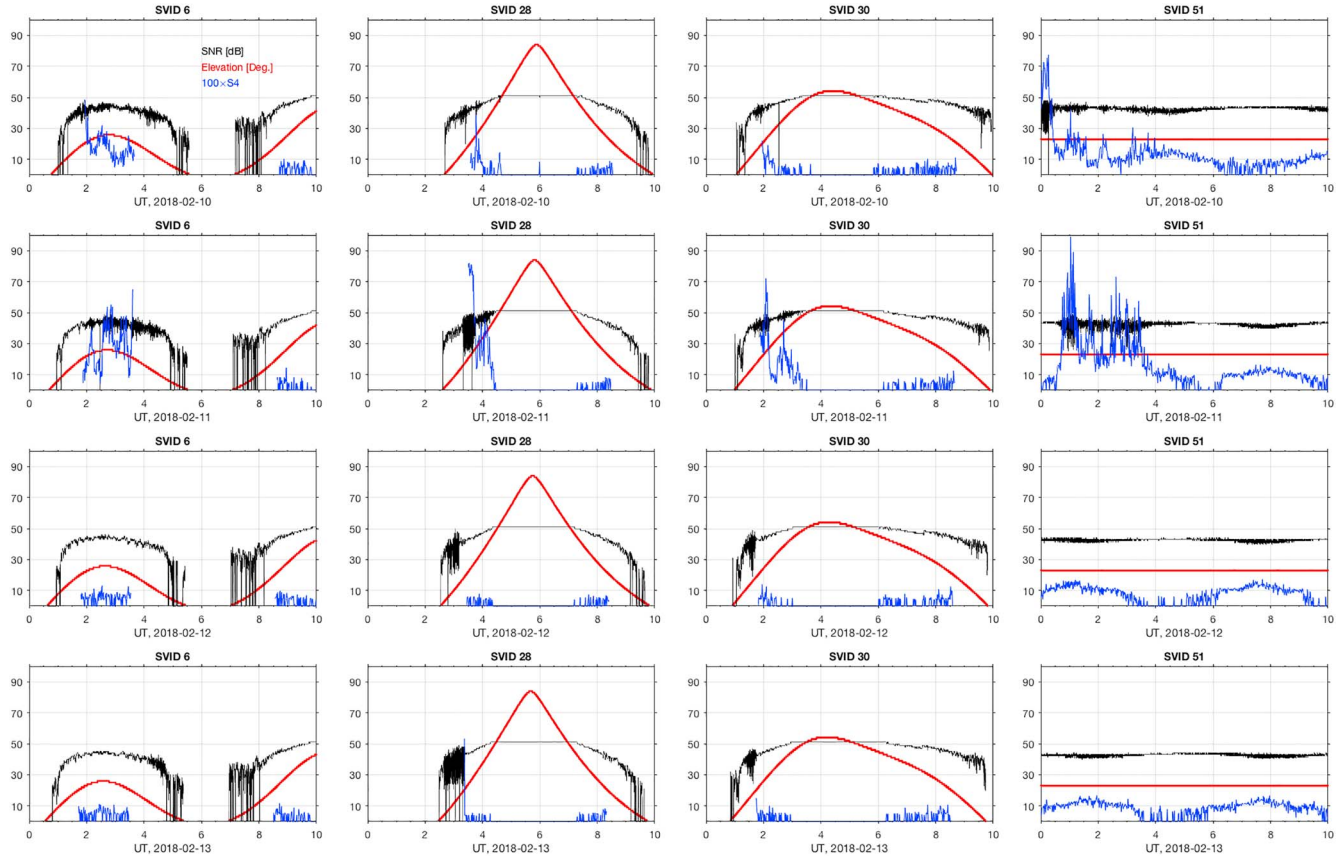

Figure 3. Expanded view of ScintPi observations for four satellites (SVIDs 6, 28, 30, and 51) on four consecutive days (10–13 February 2018). The examples illustrate that increases in the ScintPi S_4 follow well the amplitudes of the variations in signal intensity (SNR). They also exemplify the day-to-day variability in scintillation occurrence detected by ScintPi. SNR = signal-to-noise ratio.

Data from 11 February (Figure 2) summarizes observations made in a single day and illustrates a case when ScintPi captured moderate-to-strong scintillation activity. SVIDs 6, 28, 30, and 51 show maximum S_4 values ranging from 0.5 to 1.0. An expanded view of these observations is provided in Figure 3 and will be discussed in the next section. The last panel in Figure 2 shows S_4 values from all satellites on the same graph and better illustrate how the range of S_4 values vary as a function of UT. The observations on 11 January only show high S_4 values between about 01:00 and 04:00 UT, that is, between approximately 21:30 and 00:30 LT since LT to UT—3.5 hr. The start time is well within the expected time of equatorial spread *F* (ESF) irregularities reaching low latitudes based on ionosonde measurements during years of low solar flux conditions as seen in 2018 (e.g., Abdu et al., 2003). The average *F*10.7 solar flux index for 2018 was approximately 70 SFU (solar flux units).

The duration of scintillation is also in good agreement with previous studies of L-Band scintillation. It has been shown that ionosonde ESF can last throughout the night, but L-Band scintillation is mostly confined to premidnight hours. This has been attributed to the faster decay of small-scale (few hundreds of meters) irregularities responsible for L1 scintillation (Basu et al., 1978; Rodrigues et al., 2004). Another factor contributing to the lack of scintillation after midnight is the reduction in ionospheric electron density as nighttime progresses. A weakening in scintillation intensity could be expected from a reduction in the amplitude of electron density variations associated with ESF.

Figures 2 also shows that PPR ScintPi station is capable of observing the signal transmitted by the geostationary satellite Telesat Anik F1R, Wide Area Augmentation System (WAAS) SVID 51 (PRN 138), located at 107.3°W. The satellite has an elevation of 23° and azimuth of 284° with respect to the PPR site and allows for continuous ionospheric observations at a stationary ionospheric piercing point (IPP). A stationary IPP has benefits with respect to moving IPPs provided by GPS satellite signals. First, it provides uninterrupted monitoring of a single coordinate. Second, it is relatively simple to derive zonal irregularity drifts from the

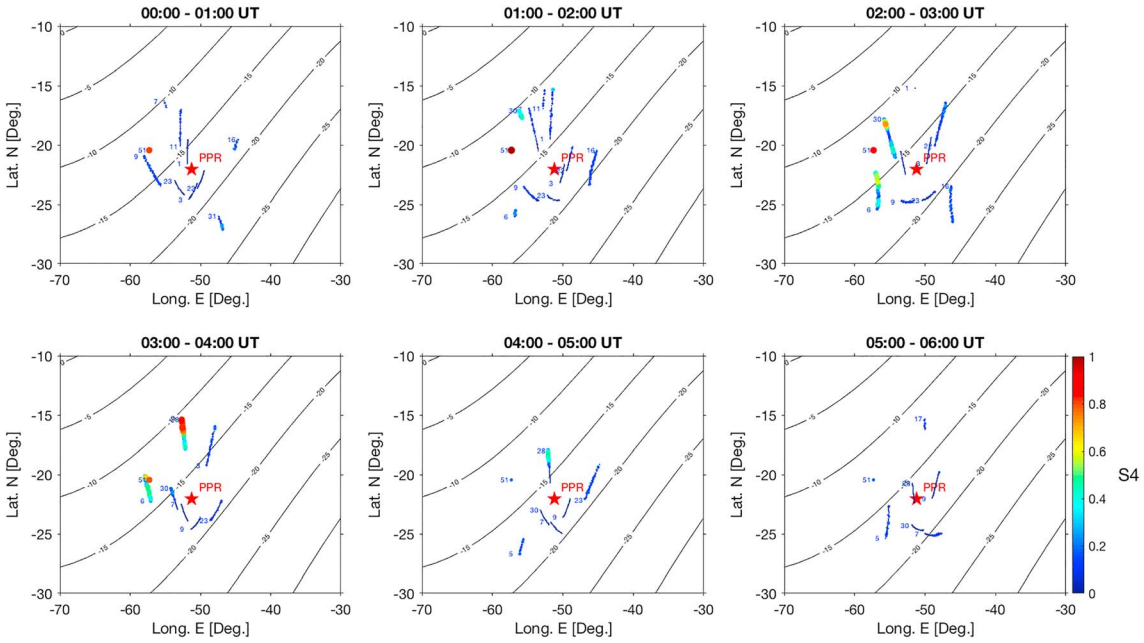

Figure 4. The spatial distribution of S_4 values observed by ScintPi on 11 February 2018. The S_4 values are represented by the color and size of the markers, which are plotted as a function of the latitude and longitude of the ionospheric piercing points. PPR = Presidente Prudente.

spaced-receiver technique (Kil et al., 2002) compared to cases when satellites are moving. While we envision the use of ScintPi data to estimate zonal irregularity drifts, this study is beyond the scope of the present report.

4.2. Observed Variations of Signal Intensity and Day-to-Day Variability

Figure 3 show more detailed examples of ScintPi observations and S_4 estimates. It shows the observations for SVIDs 6, 28, 30, and 51 on four consecutive days, between 10 and 13 January 2018. The examples in Figure 3 serve to show that, as expected, increases in S_4 values follow closely increases in signal intensity (SNR) fluctuations. The examples show fluctuations in SNR that exceed 20 dB peak to peak. See, for instance, the signal variations on SVID 51 on 11 February, which cause S_4 values to exceed 0.7 between 00:00 and 00:30 UT.

The examples of Figure 3 also serve to show the day-to-day variability in irregularity (and scintillation) occurrence near PPR. Scintillation events are observed on 10 and 11 February, but not on 12 and 13 February. Scintillation occurrence over PPR is dictated by instability growth conditions at the magnetic equator and by background conditions leading to ESF vertical development. That is, for scintillation to be observed at PPR (at −16.8° magnetic latitude), ESF needs to occur and reach a significant altitude (over >900 km) at the magnetic equator. This is based on IGRF magnetic field line mapping from an altitude of 350 km above PPR. As the ESF structure develops vertically, it also maps along geomagnetic field lines and reaches higher magnetic latitudes. In fact, we argue that, given the extremely low solar flux conditions of 2018 (F10.7–70 SFU), ESF structures would not reach the latitude of PPR very often. As a consequence, scintillation would be observed, mostly, to the (magnetic) north of the site. In the following section, we show an example of the spatial variation of S_4 indices that can be seen with ScintPi and that confirms that scintillation events occurred more frequently to the magnetic north of PPR.

4.3. Spatial Distribution of Irregularities and Scintillation

The previous sections showed that variations in signal intensity can be detected in the ScintPi measurements, despite the low resolution in time and amplitude of the SNR samples. More importantly, the observations only showed scintillation during times when ESF is expected to occur. We now turn our attention to the spatial distribution of scintillation and irregularities, which can be obtained with GPS observations such as those made by ScintPi. Figure 4 shows an example of the latitude-versus-longitude distribution of S_4 values as a function of time. Only signals from satellites with elevation greater than 20° are shown.

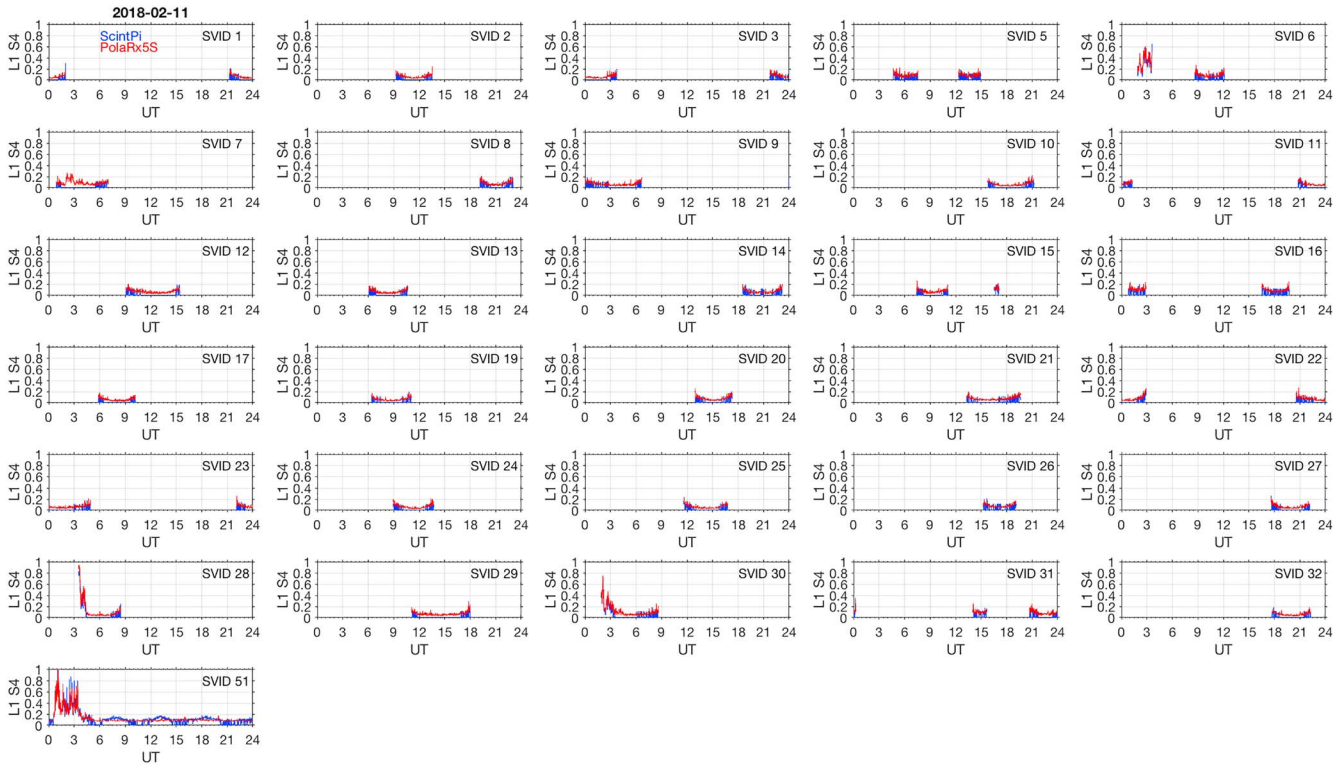

Figure 5. S_4 values estimated by ScintPi and PolaRx5S for observations made on 11 February 2018.

Figure 4 shows the ionospheric piercing points (IPPs) of the various signals observed by ScintPi on 11 February 2018, between 00:00 and 06:00 UT. Each panel shows 1 hr of data. The color and size of the markers used to track the IPPs represent the magnitude of the S_4 index. The SVID is indicated at the beginning of each track. Note that only the IPP of the WAAS signal (SVID 51) does not change with time. The IPPs were computed assuming a mean ionospheric height of 350 km. Isolines of magnetic latitude are also shown for reference.

As explained in the previous section, we expected that scintillation events would be observed with higher occurrence rates to the (magnetic) north of the site. The example of 11 February (Figure 4) confirms our expectation, showing more cases of enhanced S_4 at magnetic latitudes lower than that of PPR. Ionospheric irregularities causing high S_4 values were not observed by signals with IPPs at higher latitudes. We also observed, however, cases of moderate scintillation ($S_4 \sim 0.6$) around the same magnetic latitude of the site but to the magnetic west. This is case for SVID 6 on the panel for 02:00–03:00 UT.

4.4. Comparison With PolaRx5S

The previous section provided examples of the type of observations that can be made with ScintPi on a daily basis. These examples also provide compelling evidence that this low-cost instrument can remote sense ionospheric irregularities. Here, we provide results of a comparison of ScintPi S_4 values with those output by a specialized, commercial scintillation monitor. While the comparison serves to confirm the usefulness of our system, it also serves to identify potential limitations.

Figure 5 shows a summary of the time variation of the S_4 values derived from ScintPi and the S_4 values output by the PolaRx5S on 11 February 2018. Each panel of Figure 5 shows the S_4 values for a SVID including the S_4 for the WAAS signal (from SVID 51). We remind the reader that both receivers used the signals collected by the same antenna using a signal splitter. This was done to examine the ability of ScintPi to identify scintillation events given adequate signals. It was also done so that we could compare the ScintPi estimates against well-validated S_4 values. The results in Figure 5 show that the ScintPi S_4 values follow closely the variation (and magnitude) of the S_4 values estimated by the PolaRx5S. One can start to notice,

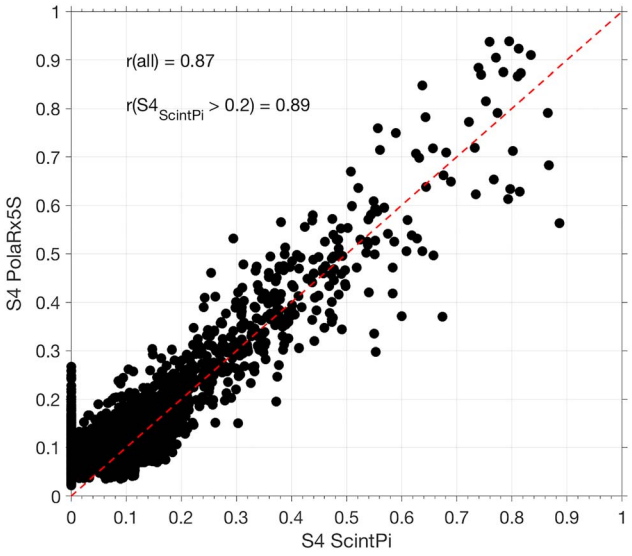

Figure 6. Linear correlation between S_4 values derived from ScintPi and S_4 values output by PolaRx5S for observations made on 11 February 2018.

however, that the values from both receivers tend to depart for $S_4 < 0.2$. This is, in most part, due to the low resolution (10 Hz and 1 dB) of the Adafruit GPS module. A better, expanded view of the observations for a few representative cases are shown in Figure 7.

In order to quantify the relationship of the ScintPi estimates with PolaRx5S outputs, we computed the linear correlation of the two S_4 values. Figure 6 shows a scatter plot of the observations for 11 February 2018 when scintillation events with S_4 values ranging from 0 to 1 were detected. Figure 6 indicates a linear correlation between the two S_4 estimates. When all the data is considered (elevation > 20°), we found a coefficient of linear correlation of about 0.87 indicating a strong positive linear correlation between the two data sets. It is clear from Figures 8 and 9, however, that ScintPi has difficulties in determining the precise value of S_4 for cases when scintillation is very weak or absent. When only ScintPi $S_4 > 0.2$ are considered in our linear correlation analysis, the correlation coefficient increases (to 0.89) but not substantially.

While the observations suggest that ScintPi performs fairly well with respect to PolaRx5S, our analyses identified at least two important limitations of the system compared to a commercial scintillation monitor. This is not surprising given that the cost of ScintPi is 2 orders of magnitude lower than that of a specialized scintillation receiver. To aid our explanation and discussion, we provided an expanded view of the observations of SVIDs 6, 7, 28, 30, and 51 between 00:00 and 10:00 UT in Figure 7. In addition to data from 11 February, we show observations made on the previous day (10 February) when moderate and strong scintillations were also observed. The examples in Figure 7 serve to better show how ScintPi S_4 values follow well the PolaRx5S values in most cases and also to highlight that ScintPi values can deviate from the "true" (PolaRx5S) values at times. Two main factors were identified in causing difficulties for ScintPi to provide accurate S_4 values.

First, as expected, the low resolution of the SNR values (1-dB steps provided by the Adafruit GPS module) cause difficulties in accurately estimating S_4. This is particularly true for small variations in signal intensity (weak scintillation). See, for instance, the S_4 values for SVID 30 between 06:00 and 08:00 UT on 10 and 11

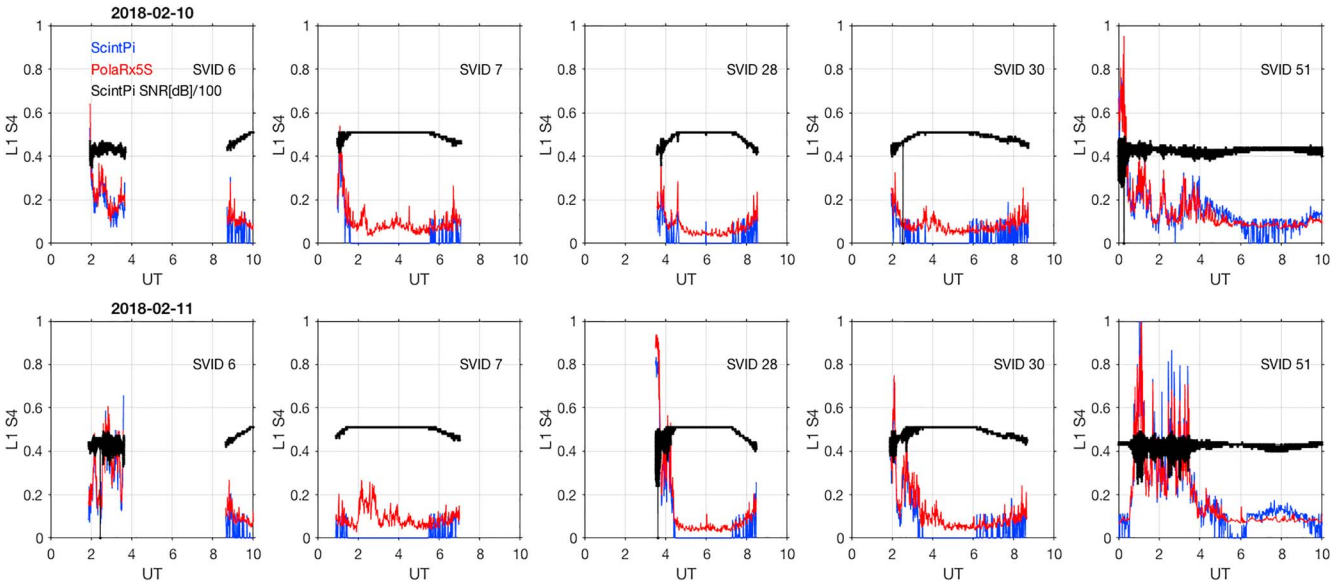

Figure 7. An expanded view of the S_4 values provided by ScintPi and PolaRx5S for 10 and 11 February 2018. The signal-to-noise ratio values provided by the Adafruit GPS module are also shown.

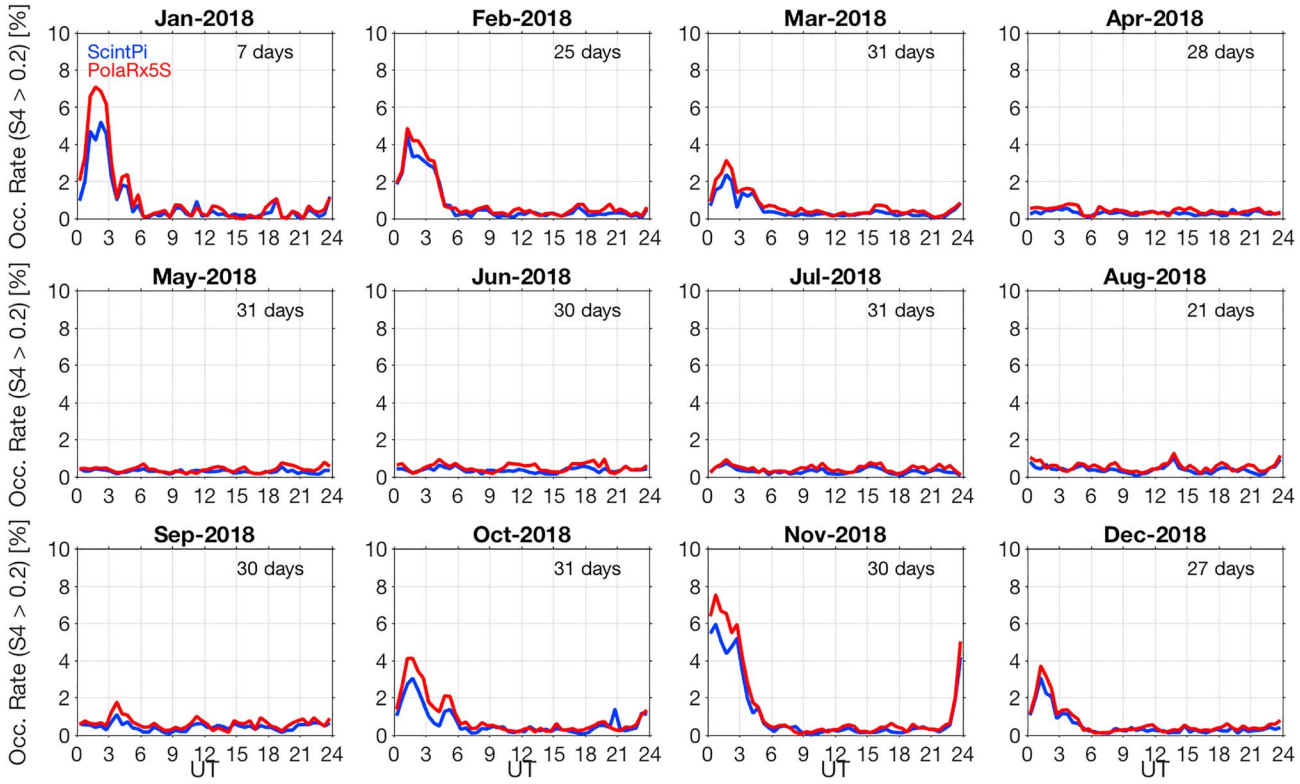

Figure 8. Occurrence rates of scintillation events with $S_4 > 0.2$ as observed by ScintPi at Presidente Prudente. Only signals from satellites with elevation greater than 20° were considered, including SVID 51 (WAAS).

February. ScintPi returns S_4 values near 0 with jumps to about 0.1, which are caused by constant values of SNR or values varying only by 1 dB within the 1-min observation time. This difficulty is not a major issue for most studies of low-latitude scintillation, where S_4 values of interest and associated with ESF are normally well above 0.2. It might be an issue, however, for studies requiring precise estimates of S_4 during weak scintillation. One example would be the monitoring of ionospheric irregularities near the magnetic equator and at high latitudes, where amplitude scintillation intensities at L-Band frequencies are typically not strong (de Paula et al., 2003; Jiao et al., 2013).

The second factor affecting the estimates of S_4 by ScintPi is a limit in the maximum SNR value provided by the Adafruit GPS module in the NMEA message. Our observations show that GPS module has a threshold value of 52 dB. This can be seen in the plots of Figure 2. For the PPR setup, this value is easily reached for satellites with moderate elevation (say, greater than 45°). See, for example, SNR and elevation values in Figure 3. This would cause ScintPi to compute erroneous S_4 values for moderate-to-strong scintillation events for signals of satellites with moderate and high elevations. It would also cause ScintPi to miss weak scintillation cases. One example of such a scenario can be seen in Figure 7, for SVID 7 on 11 February. The PolaR5Sx shows a weak event ($S_4 \sim 0.25$) between 02:00 and 03:00 UT, which is not detected by ScintPi. During that time, ScintPi shows the constant, maximum SNR value of 52 dB for the time of interest, which results in zero intensity variance and, consequently, $S_4 = 0$.

We must point out that maximum SNR values could only be easily reached in PPR because of the setup and antenna available for the observations. The PolaNt antenna used here provides better amplification of the signal than a typical, low-cost antenna setup would. Observations using simpler, less expensive antennas would move mean SNR to lower values. The use of cheaper antennas and cabling is a more realistic scenario for observational setups envisioned for ScintPi. Therefore, the effects of the maximum SNR threshold can be, at least to some extent, minimized.

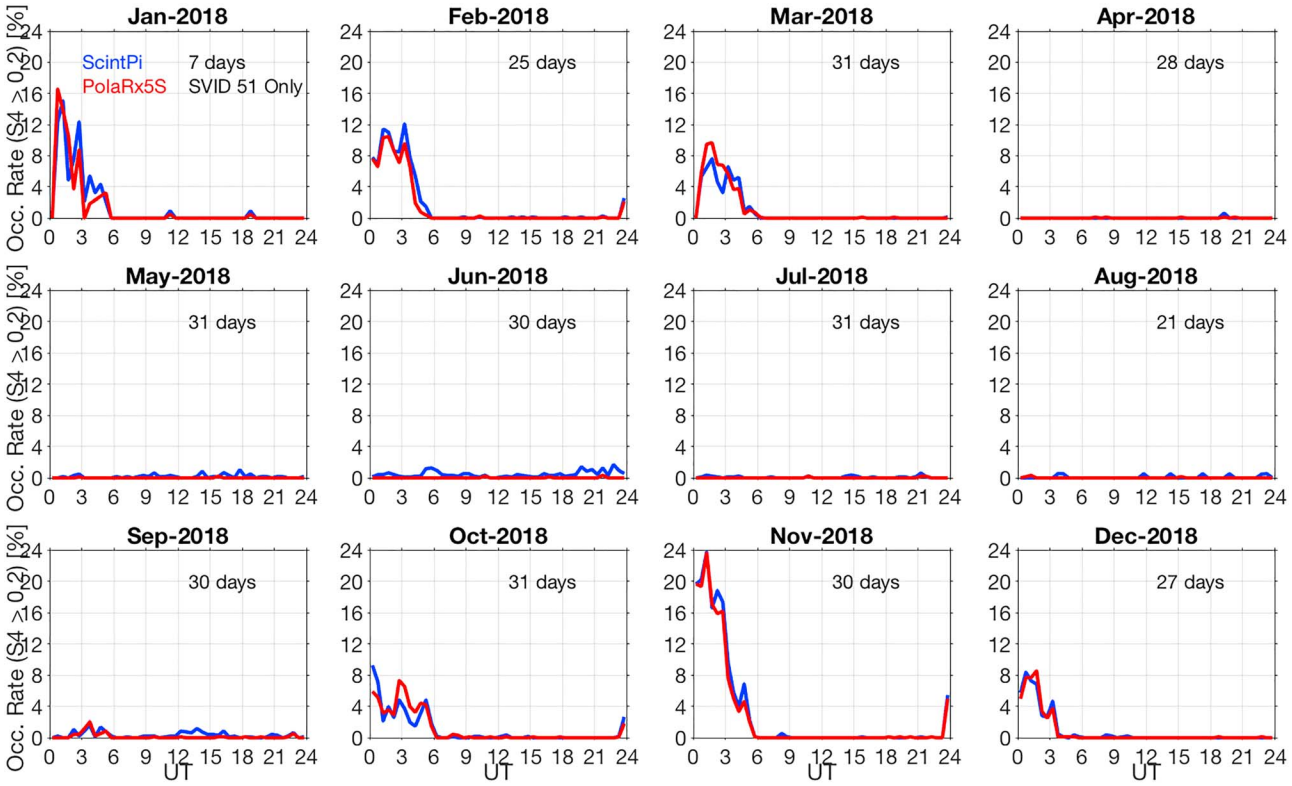

Figure 9. Occurrence rates of scintillation events with $S_4 > 0.2$ as observed by ScintPi at Presidente Prudente. Only signals from the SVID 51 (WAAS) were considered.

4.5. Long-Term Observations

Finally, we investigated the ability of ScintPi to provide long-term (1-year) information about scintillation and, therefore, information about the interannual variability of ionospheric irregularities observed from the PPR site. Figure 8 shows the hourly occurrence rates of scintillation observed by ScintPi (blue curves) for each month of 2018. For comparison, we also show the results for observations made by the PolaRx5S (red curves). The occurrence rates were obtained by computing the fraction of the total number of observations showing $S_4 > 0.2$. The occurrence rates were computed for each hour bin. Again, to avoid multipath effects, only observations from satellites with an elevation mask of 20° were used in our analyses. Also, for proper comparison, only data from days when both receivers operated were used in the analyses, and the number of days is indicated in the panels for each month.

First of all, the ScintPi results show the expected occurrence of scintillation events between September and March. ESF season in Brazil starts goes August to April (e.g., Muella et al., 2017; Sobral et al., 2002). Digisonde observations, however, show that ESF is only weak or absent during August and April at low latitudes during years of low solar activity (Abdu et al., 2003). The results in Figure 8 also show a good agreement between ScintPi and PolaRx5S. ScintPi, however, tends to show slightly lower occurrence rates than PolaRx5S during ESF season. This is the result of ScintPi missing scintillation events for high elevation satellites when SNR was truncated at 52 dB. Nevertheless, while the absolute occurrence rates differ, ScintPi is still able to capture the interannual variability in ESF. Relative variations in occurrence rates from month to month can also be observed. For instance, the increase in scintillation occurrence in November is captured by ScintPi. Even hourly variations in the occurrence rates can be identified. For instance, in October, the PolaRx5S shows a small, secondary peak around 05:00 UT. The peak is also seen in the ScintPi results.

One way to overcome the difficulties associated with the SNR threshold in ScintPi at PPR is to use signals from satellites of low elevation. One satellite in particular, WAAS SVID 51, provides interesting information. This geostationary WAAS satellite has an elevation of 23° with respect to PPR, and its signal was received

ScintPi with an average SNR of approximately 43 dB. We analyzed only the continuous signal from this geostationary satellite. Results for the monthly occurrence rates of irregularities derived from $S_4 > 0.2$ on the WAAS signal are show in Figure 9. Again, occurrence rates were obtained by computing the fraction of the total number of WAAS observations showing $S_4 > 0.2$. The occurrence rates were computed for each hour bin and for each month. Only observations made simultaneously by the ScintPi and PolaRx5S receivers were considered. The results show an excellent agreement between ScintPi and PolaRx5S for all months and local times. Small differences in occurrence rates are caused by differences in how S_4 is computed.

5. Conclusions

We presented and discussed results obtained with a low-cost, easy-to-build single-frequency GPS-based instrument (ScintPi) for monitoring ionospheric irregularities through amplitude scintillation. The system is based on the Adafruit Ultimate GPS module, which is capable of measuring, at a 10-Hz rate, the intensity of the L1 (1.575 GHz) signal.

A prototype of the system was deployed in Presidente Prudente - PPR (22.1°S, 51.24°W, −16.8° dip latitude), a low magnetic latitude site in Brazil, and observations were made throughout 2018. The deployment and observations were carried out to test the ability of the system in detecting ionospheric scintillations and, therefore, monitoring the occurrence of ionospheric irregularities. Our results show that, despite its simplicity, ScintPi is capable of detecting scintillation events associated with ESF. The system captured temporal and spatial variations in scintillation occurrence that match the expected behavior of ESF variability in the Brazilian region.

Comparison with simultaneous, collocated measurements made by a commercial GPS scintillation monitor (Septentrio PolaRx5S) was presented. The comparison allowed us to quantify the performance of the low-cost monitor and identify sources of potential limitations. The comparison confirmed that ScintPi can be used to detect ionospheric irregularities and amplitude scintillation. It showed that ScintPi provided S_4 values with a strong linear correlation (~0.87) with those output by PolaRx5S. The observations also allowed us to identify potential limitations of the system. First, the accuracy of the S_4 estimates can be affected by the low resolution (1 dB) of the SNR (intensity) values. This is particularly true for weak scintillation and might be an issue for studies that require the detection of weak scintillation and/or precise estimates of S_4 during weak scintillation events. Second, the Adafruit has a maximum SNR value of 52 dB. Such signal levels are commonly reached by satellites with moderate to high elevation (>45°) in our PPR setup. For setups with more realistic, cheaper types of antenna and cabling, we expect lower SNR levels and reduced issues with the SNR threshold.

Despite the issues with SNR resolution and threshold, we were able to use ScintPi to monitor low-latitude ionospheric irregularities for an entire year. ScintPi results follow fairly well the results obtained with Septentrio. However, at times, it underestimates monthly occurrence rates due to missing scintillation events at high elevation when the SNR is truncated at 52 dB. Using the signal from a geostationary WAAS satellite (SVID 51), which has an elevation of 23° with respect to PPR, we obtained estimates of the scintillation occurrence that are in excellent agreement with PolaRx5S. ScintPi cannot (and is not intended to) substitute commercial scintillation monitors. Instead, it has been designed and tested to be used in educational Science, Technology, Engineering, and Math (STEM) programs, scientific studies of ionospheric irregularities (space weather) that require DASI and citizen science. Confirming that the system can detect ionospheric irregularities allow us to start planning and suggesting future activities.

Educational plans include the involvement of undergraduate students from different majors in activities that will improve the system. Priority improvements include an alternative GPS module that has no limitations in SNR output and the development of real-time signal processing, uploaded to a central server and generation of quick-look online plots for public view. Students would be involved in designing the improvements and analyzing the results. Learning outcomes would include but are not limited to increasing: effective use of science and engineering principles to solve problems, effective teamwork practices, effective communication skills, and ability to organize and analyze data from multiple sources.

From a scientific perspective, we envision the use of ScintPi to provide complementary measurements to existing networks of specialized ionospheric sensors such as Low-Latitude Ionosphere Sensor Network -

(LISN) (Valladares & Chau, 2012) in South America. The significant cost of instruments (vertical radio sounders (VIPR), dual-frequency GPS receivers, and magnetometers) used in networks like LISN only allows their installation at a limited number of well-spaced observation sites. The cost of these instruments also requires adequate, well-maintained sites. The low cost of ScintPi would allow the creation of a denser distributed array of small instruments (DASI) for ionospheric irregularity studies. Such an array be useful, for instance, in studies of the morphology and behavior of ESF under different background ionospheric conditions. Digisonde and dual-frequency GPS receivers from a network like LISN could provide information about the large-scale, background ionospheric conditions. A dense ScintPi array, on the other hand, would provide information on the scintillation-producing Fresnel-scale (hundreds of meters) irregularities and their relationship to background plasma structuring. Another potential use of ScintPi is monitoring of ionospheric irregularities in Africa where the number of ionospheric sensors is small compared to South America. The ionospheric electrodynamics shows interesting characteristics in that longitude sector and ESF shows significant variability in the zonal direction within the continent (Yizengaw et al., 2012; Yizengaw et al., 2013). Deployment of ScintPi receivers could be a low-cost alternative to investigations of ionospheric irregularities in that sector while promoting education in space sciences. A dense array of ScintPi sensors is achievable, and it would provide irregularity observations with much higher spatial resolution than currently possible.

Finally, ScintPi's design is straightforward as described in this report, and the system can easily be reproduced by hobbyists and interested users (citizen scientists). These users could build copies of the system and collaborate with professional scientists in the acquisition and analyses of the observations. Such an initiative would follow the success and lessons learned from previous efforts in space weather using different types of instruments and observables (Barnard et al., 2014; Frissell et al., 2014; Knipp, 2015; Kosar et al., 2018; MacDonald et al., 2015; Perry et al., 2018).

Acknowledgments
Work at UT Dallas was supported by NSF (Awards AGS-1554926 and AST-1547048). A. O. M. was supported by CNPq Award 314043/2018-7. The PolaRx5S observations used in this study were collected as part of the CIGALA/CALIBRA Network, currently maintained by CNPq 465648/2014-2 and FAPESP 2017/50115-0. The authors would like to thank the technical support provided by Galera Monico, Italo Tsuchiya, and Marcelo Pirro from UNESP. All the ScintPi measurements (S_4 indices) made during 2018 in Presidente Prudente are available on a public repository (DOI: 10.5281/zenodo.3261804). We also made raw (10 Hz) measurements for 11 February 2018 available on the same repository. Septentrio data used in this paper are from the CIGALA/CALIBRA network and are available to be downloaded through the website (http://is-cigala-calibra.fct.unesp.br/is/index.php).

References

Aarons, J. (1982). Global morphology of ionospheric scintillations. *Proceedings of the IEEE*, *70*, 360–378.

Abdu, M. A., Souza, J. R., Batista, I. S., & Sobral, J. H. A. (2003). Equatorial spread F statistics and empirical representation for IRI: A regional model for the Brazilian longitude sector. *Advances in Space Research*, *31*(3), 703–716.

Adafruit (2018). Adafruit Learning Systems, Adafruit Ultimate GPS, https://cdn-learn.adafruit.com/downloads/pdf/adafruit-ultimate-gps.pdf.

Baker, D. N., & Lanzerotti, L. J. (2016). Resource Letter SW1: Space Weather. *American Journal of Physics*, *84*, 166. https://doi.org/10.1119/1.4938403

Barnard, L., Scott, C., Owens, M., Lockwood, M., Tucker-Hood, K., Thomas, S., et al. (2014). The Solar Stormwatch CME catalogue: Results from the first space weather citizen science project. *Space Weather*, *12*, 657–674. https://doi.org/10.1002/2014SW001119

Basu, S., Basu, S., Aarons, J., McClure, J. P., & Cousins, M. D. (1978). On the coexistence of kilometer- and meter-scale irregularities in the nighttime equatorial F region. *Journal of Geophysical Research*, *83*(A9), 4219–4226. https://doi.org/10.1029/JA083iA09p04219

Beach, T. L., & Kintner, P. M. (2001). Development and use of a GPS ionospheric scintillation monitor. *IEEE Transactions on Geoscience and Remote Sensing*, *39*, 918–928. https://doi.org/10.1109/36.921409

Bust, G. S., & Mitchell, C. N. (2008). History, current state, and future directions of ionospheric imaging. *Reviews of Geophysics*, *46*, RG1003. https://doi.org/10.1029/2006RG000212

Coupling, Energetics and Dynamics of Atmospheric Regions (2010). Coupling, Energetics and Dynamics of Atmospheric Regions: The new dimension—Strategic Plan, V9.2, October, http://cedarweb.vsp.ucar.edu/.

de Paula, E. R., Rodrigues, F. S., Iyer, K. N., Kantor, I. J., Abdu, M. A., Kintner, P. M., et al. (2003). Equatorial anomaly effects on GPS scintillations in Brazil. *Advances in Space Research*, *31*(3), 749–754, ISSN 0273-1177. https://doi.org/10.1016/S0273-1177(03)00048-6

Farley, D. T. (1991). Early incoherent scatter observations at Jicamarca. *Journal of Atmospheric and Terrestrial Physics*, *53*(8), 665–675. https://doi.org/10.1016/0021-9169(91)90120-V

Frissell, N. A., Miller, E. S., Kaeppler, S. R., Ceglia, F., Pascoe, D., Sinanis, N., et al. (2014). Ionospheric sounding using real-time amateur radio reporting networks. *Space Weather*, *12*, 651–656. https://doi.org/10.1002/2014SW001132

Isham, B., Tepley, C. A., Sulzer, M. P., Zhou, Q. H., Kelley, M. C., Friedman, J. S., & González, S. A. (2000). Upper atmospheric observations at the Arecibo Observatory: Examples obtained using new capabilities. *Journal of Geophysical Research*, *105*(A8), 18,609–18,637. https://doi.org/10.1029/1999JA900315

Jakowski, N. (1996). In H. Kohl, R. Riister, & K. Schlegel (Eds.), *TEC monitoring by using satellite positioning systems, modem ionospheric science*, (pp. 371–390). Katlenburg-Lindau, ProduServ GmbH Verlagsservice, Berlin: EGS.

Jiao, Y., Morton, Y. T., Taylor, S., & Pelgrum, W. (2013). Characterization of high-latitude ionospheric scintillation of GPS signals. *Radio Science*, *48*, 698–708. https://doi.org/10.1002/2013RS005259

Kelley, M. C. (2009). The Earth's ionosphere, plasma physics and electrodynamics (2nd ed.). Amsterdam: Elsevier. *The reference was copied from a paper from AGU JGR: Space Physics for completeness*. https://agupubs.onlinelibrary.wiley.com/doi/10.1029/2018GL079695

Kelley, M. C., Baker, K. D., Ulwick, J. C., Rino, C. L., & Baron, M. J. (1980). Simultaneous rocket probe, scintillation, and incoherent scatter radar observations of irregularities in the auroral zone ionosphere. *Radio Science*, *15*(3), 491–505. https://doi.org/10.1029/RS015i003p00491

Kil, H., Kintner, P. M., de Paula, E. R., & Kantor, I. J. (2002). Latitudinal variations of scintillation activity and zonal plasma drifts in South America. *Radio Science*, *37*(1), 1006. https://doi.org/10.1029/2001RS002468

Kintner, P. M., Ledvina, B. M., & de Paula, E. R. (2007). GPS and ionospheric scintillations. *Space Weather*, *5*, S09003. https://doi.org/10.1029/2006SW000260.

Knipp, D. J. (2015). Space Weather and Citizen Science. *Space Weather*, *13*, 97–98. https://doi.org/10.1002/2015SW001167.

Kosar, B. C., MacDonald, E. A., Case, N. A., & Heavner, M. (2018). Aurorasaurus database of real-time, crowd-sourced aurora data for space weather research. *Earth and Space Science*, *5*, 970–980. https://doi.org/10.1029/2018EA0004540

MacDonald, E. A., Case, N. A., Clayton, J. H., Hall, M. K., Heavner, M., Lalone, N., et al. (2015). Aurorasaurus: A citizen science platform for viewing and reporting the aurora. *Space Weather*, *13*, 548–559. https://doi.org/10.1002/2015SW001214

Makela, J. J. (2006). A review of imaging low-latitude ionospheric irregularity processes. *Journal of Atmospheric and Solar - Terrestrial Physics*, *68*, 1441–1458. https://doi.org/10.1016/j.jastp.2005.04.014

Moraes, A. O., Costa, E., Abdu, M. A., Rodrigues, F. S., de Paula, E. R., Oliveira, K., & Perrella, W. J. (2017). The variability of low-latitude ionospheric amplitude and phase scintillation detected by a triple-frequency GPS receiver. *Radio Science*, *52*, 439–460. https://doi.org/10.1002/2016RS006165

Moraes, A. O., Muella, M. T. A. H., de Paula, E. R., de Oliveira, C. B. A., Terra, W. P., Perrella, W. J., & Meinbach-Rosa, P. R. P. (2017). Statistical evaluation of GLONASS amplitude scintillation over low latitudes in the Brazilian territory. *Advances in Space Research*, *61*(7), 1776–1789. https://doi.org/10.1016/j.asr.2017.09.032

Moraes, A. O., Vani, B. C., Costa, E., Sousasantos, J., Abdu, M. A., Rodrigues, F., et al. (2018). Ionospheric scintillation fading coefficients for the GPS L1, L2, and L5 frequencies. *Radio Science*, *53*, 1165–1174. https://doi.org/10.1029/2018RS006653

Muella, M. T. A. H., Duarte-Silva, M. H., Moraes, A. O., de Paula, E. R., Rezende, L. F. C., Alfonsi, L., & Affonso, B. J. (2017). Climatology and modelling of ionospheric scintillations and irregularity zonal drifts at the equatorial anomaly region. *Annales Geophysicae*, *35*, 1201–1218. https://doi.org/10.5194/angeo-35-1201-2017

National Research Council (2006). *Distributed arrays of small instruments for solar-terrestrial research: Report of a workshop*. Washington, DC: The National Academies Press. https://doi.org/10.17226/11594

Perry, G. W., Frissell, N. A., Miller, E. S., Moses, M., Shovkoplyas, A., Howarth, A. D., & Yau, A. W. (2018). Citizen radio science: An analysis of amateur radio transmissions with e-POP RRI. *Radio Science*, *53*, 933–947. https://doi.org/10.1029/2017RS006496

Rino, C. L., Tsunoda, R. T., Petriceks, J., Livingston, R. C., Kelley, M. C., & Baker, K. D. (1981). Simultaneous rocket-borne beacon and in situ measurements of equatorial spread F—Intermediate wavelength results. *Journal of Geophysical Research*, *86*(A4), 2411–2420. https://doi.org/10.1029/JA086iA04p02411

Rodrigues, F. S., de Paula, E. R., Abdu, M. A., Jardim, A. C., Iyer, K. N., Kintner, P. M., & Hysell, D. L. (2004). Equatorial spread F irregularity zcharacteristics over São Luís, Brazil, using VHF radar and GPS scintillation techniques. *Radio Science*, *39*, RS1S31. https://doi.org/10.1029/2002RS002826

Skone, S., Knudsen, K., & de Jong, M. (2001). Limitations in GPS receiver tracking performance under ionospheric scintillation conditions. *Physics and Chemistry of the Earth, Part A: Solid Earth and Geodesy*, *26*(6–8), 613–621, 1464-1895. https://doi.org/10.1016/S1464-1895(01)00110-7

Sobral, J. H. A., Abdu, M. A., Takahashi, H., Taylor, M. J., de Paula, E. R., Zamlutti, C. J., et al. (2002). Ionospheric plasma bubble climatology over Brazil based on 22 years (1977–1998) of 630 nm airglow observations. *Journal of Atmospheric and Solar - Terrestrial Physics*, *64*(12-14), 1517–1524. https://doi.org/10.1016/S1364-6826(02)00089-5

Tinsley, B. A., & Bittencourt, J. A. (1975). Determination of F region height and peak electron density at night using airglow emissions from atomic oxygen. *Journal of Geophysical Research*, *80*(16), 2333–2337. https://doi.org/10.1029/JA080i016p02333

Valladares, C. E., & Chau, J. L. (2012). The low-latitude ionosphere sensor network: Initial results. *Radio Science*, *47*, RS0L17. https://doi.org/10.1029/2011RS004978

Vani, B. C., Shimabukuro, M. H., & Monico, J. F. G. (2016). Visual exploration and analysis of ionospheric scintillation monitoring data: The ISMR query tool. *Computers & Geosciences*, *104*, 125–134. https://doi.org/10.1016/j.cageo.2016.08.022

Yeh, K. C., & Liu, C.-H. (1982). Radio scintillations in the ionosphere. *Proceedings of the IEEE*, *70*, 4.

Yizengaw, E., Doherty, P., & Fuller-Rowell, T. (2013). Is space weather different over Africa, and if so, why? An AGU Chapman Conference Report. *Space Weather*, *11*, 389–391. https://doi.org/10.1002/swe.20063

Yizengaw, E., Zesta, E., Moldwin, M. B., Damtie, B., Mebrahtu, A., Valladares, C. E., & Pfaff, R. F. (2012). Longitudinal differences of ionospheric vertical density distribution and equatorial electrodynamics. *Journal of Geophysical Research*, *117*, A07312. https://doi.org/10.1029/2011JA017454